Gadolinium-Incorporated Carbon Nanodots for T1-weighted Magnetic Resonance Imaging

Ding-Kun Ji, Giacomo Reina, Hanyu Liang, Da Zhang, Shi Guo, Belén Ballesteros, Cécilia Ménard-Moyon, Juan Li, Alberto Bianco

Gadolinium-Incorporated Carbon Nanodots for T_1-weighted Magnetic Resonance Imaging

Ding-Kun Ji,[1,#] Giacomo Reina,[1] Hanyu Liang,[2] Da Zhang,[2] Shi Guo,[1] Belén Ballesteros,[3] Cécilia Ménard-Moyon,[1] Juan Li,[2,#] Alberto Bianco[1,]*

[1]CNRS, Immunology, Immunopathology and Therapeutic Chemistry, UPR 3572, University of Strasbourg, ISIS, 67000 Strasbourg, France
[2]MOE Key Laboratory for Analytical Science of Food Safety and Biology, Fujian Provincial Key Laboratory of Analysis and Detection Technology for Food Safety, State Key Laboratory of Photocatalysis on Energy and Environment, College of Chemistry, Fuzhou University, Fuzhou 350116, China
[3]Catalan Institute of Nanoscience and Nanotechnology (ICN2), CSIC and the Barcelona Institute of Science and Technology, Campus UAB, 08193 Bellaterra, Barcelona, Spain

Current address: [#] Institute of Molecular Medicine (IMM), Renji Hospital, School of Medicine, Shanghai Jiao Tong University, Shanghai 200240, China

Correspondance: a.bianco@ibmc-cnrs.unistra.fr

ABSTRACT

The design and the development of contrast agents for magnetic resonance imaging (MRI), with improved chemical stability and higher contrasting capability for clinical translation, compared to conventional contrast agents, is still of great interest. In this study, a facile and universal approach was explored for controllable functionalization of red-emissive carbon nanodots (RCNDs) with diethylenetriaminepentaacetic anhydride (DTPA) for chelation of gadolinium. A series of accurate characterizations were used to control each step of the synthesis. The functionalization did not alter the band gap of the carbon nanodots, preserving their inherent far-red fluorescence. The as-prepared RCND-DTPA-Gd displayed a high colloidal stability with negligible Gd leakage. The nanodots showed also a better magnetic resonance relaxivity than commercial MRI agents. RCND-DTPA-Gd owned good biocompatibility *in vivo* even at high doses. Systemically injected RCND-DTPA-Gd were found to be efficiently excreted through the renal route, a feature that further minimizes potential toxicity risks. All these properties suggest that carbon nanodots can be well designed as efficient carriers of Gd, resulting in potential clinical tools as dual MRI/fluorescence functional probes for imaging applications. The approach described here could pave the pathway to a flexible strategy for controllable functionalization of small-size nanoparticles including carbon dots, rendering them more versatile. This work is expected to promote future translation of carbon nanodots into clinical trials.

KEYWORDS： carbon nanomaterials; graphene; contrast agents; fluorescence imaging; theranostics

INTRODUCTION

MRI is considered one of the most practical technique for diagnosis and medical research.[1] This technique has different advantages including non-invasiveness, elevated spatial and temporal resolution, and favorable contrast in soft tissues. For these reasons, MRI is the method of choice for imaging brain and central nervous system, for evaluating cardiac functions, and for identifying tumors.[1, 2] To increase the signal differences between normal tissues and lesions, MRI contrast agents containing gadolinium (III) are generally used in hospitals. Nevertheless, gadolinium is toxic as free ions.[3] Hence, gadolinium agents used in clinics are all in the form of complexes that chelate this element, such as Gd-DTPA (Magnevist) and Gd chelated to 1,4,7,10-tetraazacyclododecane-1,4,7,10-tetraacetic acid (DOTA) (Dotarem) to minimize toxicity. However, some studies have indicated that gadolinium may be decomplexed *in vivo*, causing severe nephrogenic systemic fibrosis, especially to patients suffering of renal diseases or with impaired renal functions.[3-5] Therefore, developing alternative MRI contrast agents with better contrasting abilities and minimized Gd leakage, is still of great interest.

Recent progresses in nanotechnology has permitted to develop new types of MRI probes made of nanoparticles.[6] One of the examples combines two single T_1 and T_2 imaging capabilities into one moiety allowing to reduce the dose and the potential toxicity.[6-9] Another widely-used method is to anchor small Gd chelating agents on the surface of the nanoparticles or to load Gd inside the holes of the nanostructures. This method enhances the potential relaxation time by raising the number of gadolinium atoms per unit volume, leading to an increased T_1 relaxivity and to reduced dose of contrast agent necessary for the relaxation of the protons.[10] Many nanosized carriers have been employed to load Gd chelates,[11] including silica nanoparticles,[12-14] polymers,[15] and carbon materials.[16-19] The nanoparticle-based T_1 contrast agents not only owned increased circulation time, but they also demonstrated a positively enhanced contrast effect.[10] However, because of their relatively large dimension (>100 nm), these nanoparticles largely accumulate in the organs of the reticuloendothelial system after systemic injection, making their long-term effect on the host organism still widely unknown. Besides that, a high colloidal stability is needed for *in vivo* administration of a MRI agent. Unfortunately, these nanoparticles usually have a hydrophobic surface, and complicated chemical processes are needed to make them hydrophilic and thus stable in physiological environments. Therefore,

uniformly small nanosized carriers with high colloidal stability, good Gd loading and minimal toxicity are still demanded as MRI agent for clinical translation.

Carbon nanodots (CNDs), the new class of luminescent quantum dots, have been intensely studied since their discovery in 2004.[20] CNDs are environmental friendly candidates aiming at substituting both organic dyes and semiconducting quantum dots in biomedicine and bioimaging, as they display many advantages like low toxicity, excellent biocompatibility, superior luminescence performances and chemical stability.[21] Thanks to their superior luminescence, such as high quantum yield, photostability, CNDs have been widely used for fluorescence imaging both *in vitro* and *in vivo*.[22, 23] Additionally, because these nanomaterials have a size below 10 nm, they can be efficiently eliminated through the kidneys.[24] Benefitting from the presence of rich reactive functions on their surface, the properties of CNDs can be precisely tuned through a controlled chemical modification. Previous studies explored different approaches to synthesize CNDs for MRI.[25-27] For example, Xu *et al.* prepared magnetic CNDs by a hydrothermal method through mixing carbon precursors with gadolinium, the metal being therefore embedded within the CND structure. This is an interesting approach, but the possibility of further chemically modifying the CNDs and how this would affect the CND properties were not explored. In addition, we think that the control and the reproducibility of the synthesis might be an issue. Integrating their superior luminescence, Gd-CND conjugates were also designed for multimodal imaging.[28-30] Different noncovalent and covalent chemical strategies have been used to modify CNDs. Noncovalent approaches have the drawback of blocking the loading capacity of CNDs and decreasing the opportunity of further functionalization. Moreover, the stability of the noncovalent complexes is often very low, with risk of release of the chelated metal before reaching the target. Recently, cyclic DTPA dianhydride (cDTPAA) was covalently linked to the surface of nitrogen-doped carbon dots to chelate Gd, resulting in stable nanoparticles for MRI.[30, 31] However, there is a risk of cDTPAA hydrolysis during the coupling reaction, which usually brings undesirable conjugates.[32] Thus, controlled covalent modification strategies for CNDs are still highly desired in the context of CND-based MRI agents for clinical use.

Here, we report a straightforward method for the covalent functionalization of RCNDs with DTPA, followed by chelation with gadolinium for T_1-weighted MRI. We proved that RCND-DTPA-Gd displayed a high colloidal stability in physiological

conditions with negligible Gd leakage, maintained a high fluorescence emission, and exhibited a better magnetic resonance relaxivity than commercial MRI agents. Remarkably, the carrier RCND-DTPA showed no toxicity to mice and did cause no damage to kidney or other organs. Systemically injected RCND-DTPA-Gd were found to be efficiently excreted through the renal route, a feature that further minimizes toxicity. All these properties suggested that DTPA-modified RCNDs are efficient carriers for Gd with a great potential as clinical probes for MRI/fluorescence functional imaging. In comparison to previous works, we have developed a synthetic strategy that is versatile to modify carbon nanodots and allows to maintain the fluorescence properties of the dots. It is based on the covalent conjugation of DTPA that is able to complex different types of metals.

RESULTS AND DISCUSSION

Design, synthesis and characterization of RCND-DTPA-Gd

RCNDs functionalized with DTPA were synthesized using a four-step procedure (Scheme 1). First, pristine RCNDs with a size below 5 nm were obtained from the hydrothermal treatment of a conjugated polythiophene phenylpropionic acid (PPA) polymer according to our previous work.[33] Exploiting the presence of the high amount of carboxylic groups on their surface, RCNDs were covalently conjugated to the DTPA derivative containing a free amine through carbodiimide chemistry (Scheme 1). The *tert*-butyl ester protecting groups were subsequently removed using trifluoroacetic acid (TFA) to prepare RCND-DTPA. Finally, RCND-DTPA-Gd were obtained by dispersing the RCND-DTPA in a water solution of gadolinium(III) perchlorate, followed by dialysis in distilled water to remove free gadolinium ions. The most popular way to conjugate DTPA to nanoparticles generally involves the amidation reaction of one of the four equivalent carboxylic groups. Apart from being non-selective, this method has the handicap of affording conjugates with a sensibly lower chelating ability compared to free DTPA.[34] In this work, a DTPA derivative bearing five free COOH groups was prepared to maximize the chelating capacity of DTPA for gadolinium (see SI for details).[19, 35]

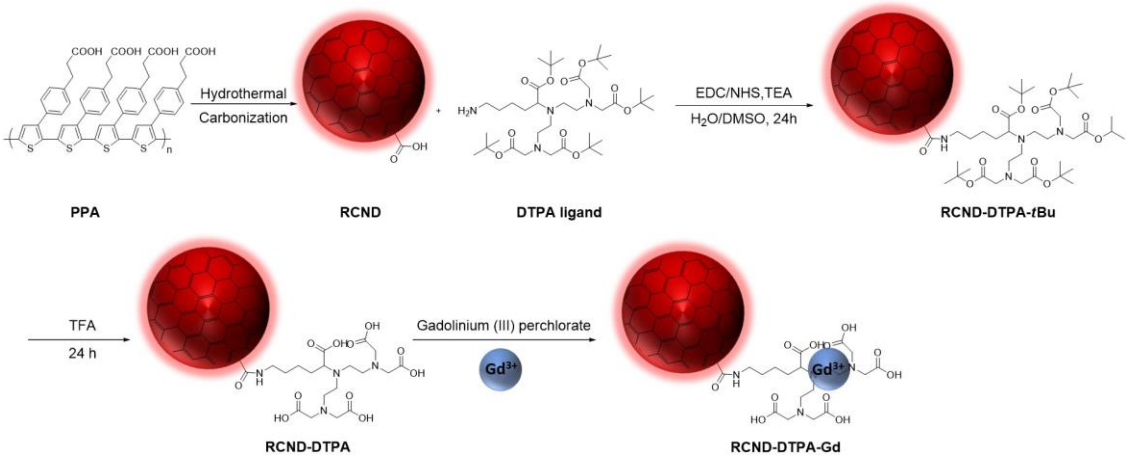

Scheme 1. Synthesis of RCND-DTPA-Gd.

The RCNDs and RCND-DTPA conjugates were characterized by high-resolution transmission electron microscopy (HRTEM), FT-IR, X-ray photoelectron spectroscopy (XPS) and thermogravimetric analysis (TGA). HRTEM images allowed to measure the size of pristine RCNDs with rough edges below 5 nm (Figure 1a), while RCND-DTPA displays a nearly smooth round shape (Figure 1b). We can observe that there are negligible differences between the HRTEM image of the RCNDs and the core of RCND-DTPA, suggesting that the RCND structure was preserved after the chemical treatments. Their size distribution was also measured using dynamic light scattering (DLS). Both RCNDs and RCND-DTPA exhibited homogenous and narrow size distribution in solution, corresponding to 2-5 nm for RCNDs and 5-11 nm for RCND-DTPA with an average diameter of 2.9 and 7.5 nm, respectively (Figure 1c). The increased nanoparticle size is attributed to the successful modification with DTPA ligand. Compared to RCNDs, FT-IR spectroscopy allowed to identify the N-H and the amide I stretching at 3296 cm^{-1} and 1637 cm^{-1}, respectively (Figure 1d). The increased shoulder around 1720 cm^{-1} confirmed the presence of the C=O stretching of carboxylic groups. XPS analysis of RCND-DTPA shows the additional peak of nitrogen, which is a further proof of the conjugation with DTPA ligand (Figure 1e). These results jointly confirm that DTPA chelating molecule was covalently bound to the surface of RCNDs. The amount of DTPA ligand on the RCNDs was calculated by TGA performed in N_2 atmosphere (Figure 1f). TGA of RCND-DTPA exhibited an increase of weight loss of 22% at 500°C in comparison to starting RCNDs, corresponding to 440 µmol/g of functional groups.

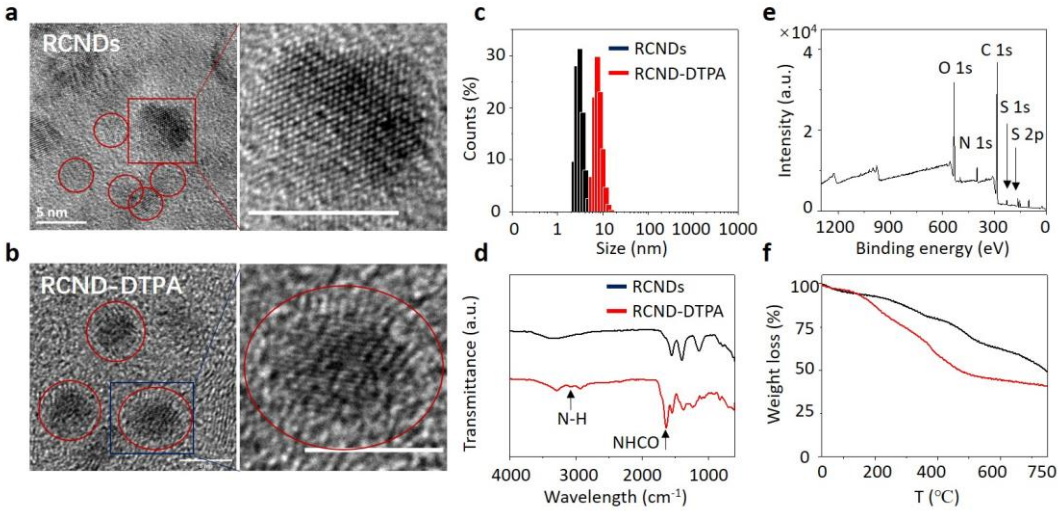

Figure 1. HRTEM images of a) RCNDs and b) RCND-DTPA (the red circles show edges of nanoparticles, the scale bar is 5 nm); c) DLS and d) FT-IR spectra of RCNDs and RCND-DTPA; e) XPS survey spectra of RCND-DTPA; f) Thermogravimetric analyses of RCNDs (black line) and RCND-DTPA (red line).

Following the complexation with Gd, the RCND-DTPA-Gd conjugate was characterized by high angle annular dark field (HAADF)-STEM, energy dispersive X-ray spectroscopy (EDX), electron energy loss spectroscopy (EELS), inductively coupled plasma atomic emission spectrometry (ICP/AES) and XPS. HAADF-STEM is a valid microscopy technique for the direct imaging of heavy-elements combined with organic molecules down to the atomic scale. The signal intensity is proportional to the atomic number of the element present in the sample. In the HAADF-STEM images of RCND-DTPA-Gd, many well-dispersed bright dots corresponding to the carbon nanodots were observed (Figure 2a and S1). EDX and EELS analyses corroborated the presence of gadolinium on the nanodots (Figure 2b and 2c). Then STEM-EELS spectral imaging was performed to localize Gd on the sample at the nanometer level. The compositional maps shown in Figure 2a proved that gadolinium was located only on the carbon nanodots, whereas carbon was present both on the nanodots and on the TEM grid carbon support, confirming the successful complexation of RCND-DTPA with Gd. The structure of RCND-DTPA-Gd was further investigated by XPS analysis (Figure 2d). The typical peaks equivalent to C 1s (284.9 eV), N 1s (398.1 eV), O 1s (530.6 eV), S 1s (228.4 eV), and Gd 3d (1187 eV) and Gd 4d (143 and 148 eV) were observed in the XPS survey spectrum, confirming that RCND-DTPA-Gd were primarily composed of C, N, O, S and Gd (Figure 2d-f).

The presence of two Gd 4d and Gd 3d peaks supported the fact that the oxidation state of Gd in RCND-DTPA-Gd remained trivalent.[24] Furthermore, ICP/AES of RCND-DTPA-Gd allowed to obtain the amount of functional groups, corresponding to 586±4 µmol of gadolinium per gram of nanoparticles. We further calculated that there is one atom of Gd every 90 C atoms (see detailed in Materials and Methods). The loading value of Gd (586 $\mu mol \cdot g^{-1}$) is a little higher than that of DTPA obtained from TGA. Nevertheless, the two loading numbers are of the same order of magnitude. It is worth noting that ICP/AES is much more precise than TGA, which is more appropriate for comparing samples before and after functionalization to confirm that the conjugation of molecules occurs rather than giving a precise loading value.

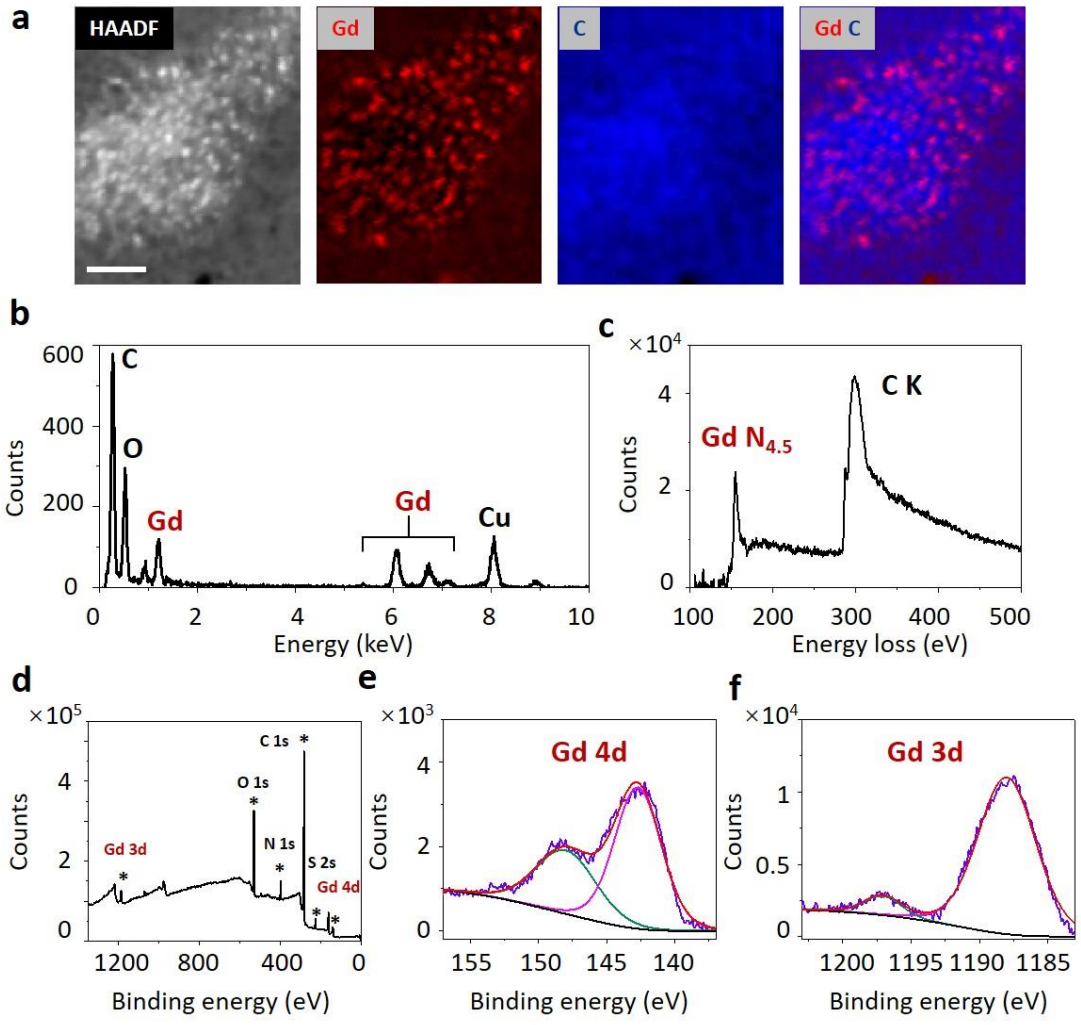

Figure 2. a) HAADF-STEM image of RCND-DTPA-Gd (the scale bar is 20 nm) and STEM-EELS mapping of Gd (in red) and C (in blue) on the same area confirming that the Gd is located on the carbon nanodots. b) EDX spectrum of RCND-DTPA-Gd

showing the presence of gadolinium. c) A typical background subtracted EEL spectrum on the sample displaying the Gd $N_{4,5}$ and C K edges. d) XPS spectra of survey, e) Gd 4d, and f) Gd 3d of RCND-DTPA-Gd.

Dispersibility and stability of RCND-DTPA and RCND-DTPA-Gd

A proper evaluation of the biological applications of nanoparticles requires their high colloidal stability in aqueous media. Both RCND-DTPA and RCND-DTPA-Gd were easily dispersed in water, PBS, saline and cell culture medium, and exhibited a lasting stability (over weeks) without evident precipitation at room temperature (Figure 3a). The stability of RCND-DTPA and RCND-DTPA-Gd was scrutinized by the measurement of zeta-potential. Both conjugates showed a strong negative surface charge (Figure 3b). The surface conjugation with DTPA decreased the charge density of RCNDs from -35 to -57 mV, indicating that the attachment of DTPA can improve the dispersibility of RCNDs. After conjugation with Gd, RCND-DTPA-Gd still maintained a strong negative charge (-40 mV), ensuring a good colloidal stability. The coordination with Gd did not induce aggregation of the hydrophilic RCND-DTPA. DLS confirmed that the as-prepared RCND-DTPA-Gd displayed a narrow hydrodynamic radius distribution with an average size of ~20 nm (Figure S2).

UV-Visible-NIR and fluorescence spectroscopy of RCND-DTPA-Gd

With the RCND-DTPA and RCND-DTPA-Gd in hand, their optical properties were characterized by UV-Vis-NIR and photoluminescence (PL) spectroscopy. Both RCND-DTPA and RCND-DTPA-Gd (25 $\mu g \cdot mL^{-1}$) have a broad absorption band between 200 and 600 nm, with two characteristic peaks at 460 nm and 540 nm (Figure 3c). The spectra resemble that of RCNDs, suggesting the band gap transitions of the dots is not affected by the chemical modifications. Figure 3d shows the fluorescence spectra of RCNDs, RCND-DTPA and RCND-DTPA-Gd in PBS buffer. All samples are characterized by a wide fluorescence emission spanning the range between 500 and 800 nm, with a strong peak at 640 nm (λ_{ex} 465 nm). RCND-DTPA showed a much stronger fluorescence band, being ~six-fold higher than the emission of RCNDs in PBS (at 25 $\mu g \cdot mL^{-1}$). The enhancement of RCND fluorescence is clearly due to the surface modification as also observed in our previous findings.[33] After chelation with Gd, the fluorescence of RCND-DTPA slightly decreased, remaining still four times higher than that of the RCNDs. Being RCND-DTPA-Gd highly fluorescent, they can

be excited by light in a large range of wavelengths to emit strong photoluminescent signals (Figure 3e). We measured the fluorescence quantum yield of RCND-DTPA-Gd using a spectrophotometer connected to an integrating sphere, obtaining 0.72% in water. The excitation-independent emission behavior makes these nanodots highly performant for bioimaging (no signal overlapping).

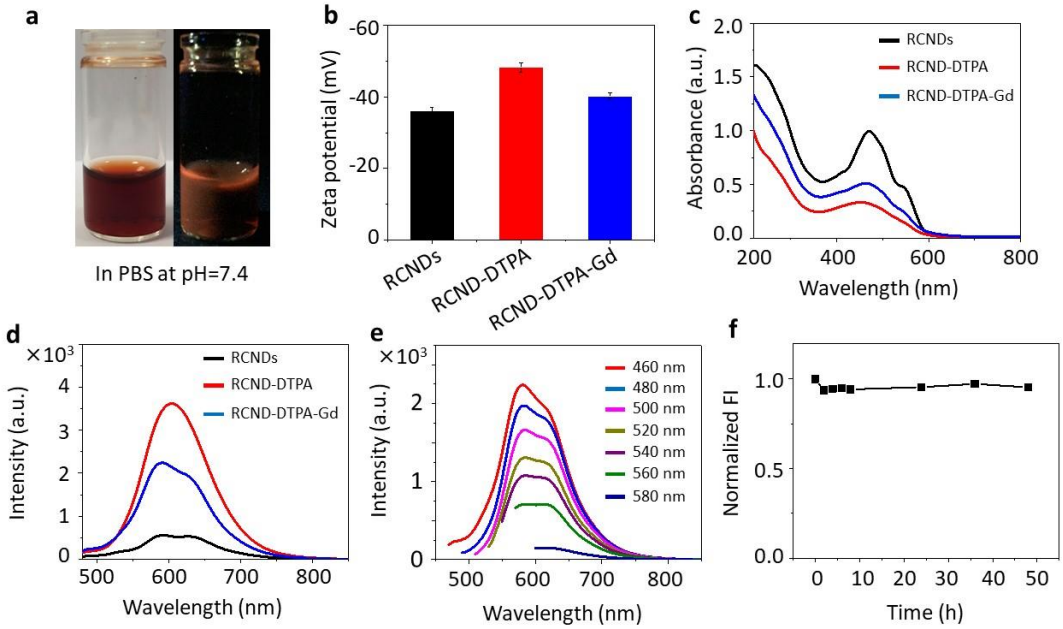

Figure 3. a) Digital image of RCND-DTPA-Gd (1 mg mL^{-1}) in PBS under sunlight (left) or under UV irradiation at 365 nm (right); b) Zeta-potential, c) UV-Vis-NIR and d) fluorescence spectra of RCNDs, RCND-DTPA and RCND-DTPA-Gd (25 μg·mL^{-1} in PBS, pH=7.4); e) Fluorescence spectra of RCND-DTPA-Gd for different excitation wavelengths; f) Normalized fluorescence intensity (FI) of RCND-DTPA-Gd (25 μg·mL^{-1}) over 48 h.

Leakage of Gd and cytotoxicity of RCND-DTPA-Gd

Taking into consideration that free gadolinium ions can trigger severe cytotoxic effects (such as cardiovascular toxicity and neurotoxicity) by inhibiting the formation of Ca^{2+} ion channels, the Gd release from the nanoparticles was investigated. RCND-DTPA-Gd were incubated at pH= 7.4 in PBS at room temperature, and their fluorescence was measured for a long period, showing no drop of luminescence intensity over 48 h (Figure 3f and S3). Moreover, if a leakage of Gd would occur, we would expect a variation of the fluorescence spectrum and a rise of the fluorescence intensity as shown in Figure 3d. Furthermore, RCND-DTPA-Gd cytotoxicity was

investigated by incubating HeLa cells with different concentrations of the conjugate (0-100 μg·mL^{-1}). The cell viability was quantified after 24 h incubation using PrestoBlue test (30 min). The RCND-DTPA-Gd exhibited no cytotoxicity against the HeLa cells in this range of concentrations (Figure S4).

Cell uptake and fluorescence imaging of RCND-DTPA-Gd

To study the cellular uptake capacity of RCND-DTPA-Gd, HeLa cells were treated with the conjugate at the concentration of 50 μg·mL^{-1} for different times (0, 4, 8, and 24 h). Benefitting from their emission in the red spectrum, RCND-DTPA-Gd were easily visualized by confocal microscopy in the NIR channel (665-715 nm). CellMask green dye was used to stain and observe the morphology of the cell membranes. Cellular uptake and fluorescence imaging of RCND-DTPA-Gd at different time points are illustrated in Figure 4. RCND-DTPA-Gd displayed a stable NIR fluorescent signal in the cell culture media. The aim of this investigation was to corroborate if the RCND-DTPA-Gd could be internalized by cells and if their fluorescent signal was stable inside the cells. Using live imaging characterization, we saw that the cell uptake of the nanodots starts in the first 4 h and that the cellular uptake increased over time up to 24 h. These data indicated that the internalization of RCND-DTPA-Gd can be mediated by endocytosis due to their small dimension and good biocompatibility.[36] The high photostability and NIR emission make RCND-DTPA-Gd a potential nanoprobe for imaging *in vitro* and *in vivo*.

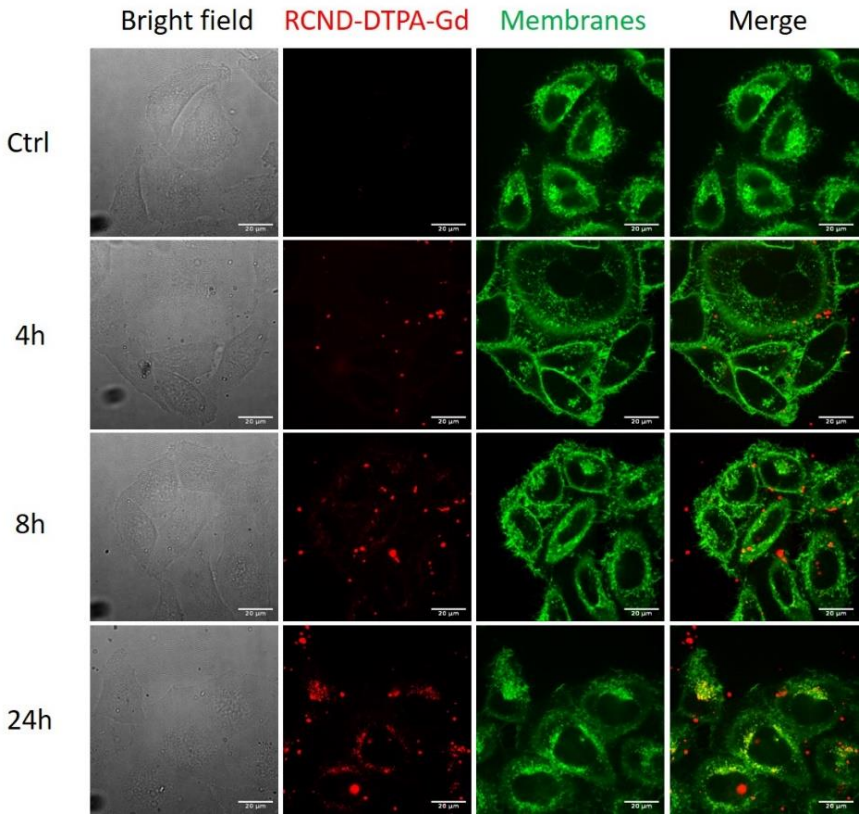

Figure 4. Confocal microscopy images on live HeLa cells incubated with 50 μg·mL^{-1} of RCND-DTPA-Gd after 4, 8, and 24 h. Cell membranes are stained in green with CellMask (excitation channel: 488 nm, emission: 500-550 nm); RCND-DTPA-Gd are stained in red (excitation channel: 405 nm, emission: 665-715 nm). The scale bar is 20 μm.

Magnetic characterization

To prove the potential applications of RCND-DTPA-Gd as contrast agent for MRI, we recorded T_1 relaxation time and T_1-weighted magnetic resonance images at different Gd concentrations using a 7 T MRI scanner. Figure 5a displays color-scaled T_1-weighted MR images, while Figure 5b represents the linear plot of the relaxation rates versus the equivalents of Gd concentration (Table 1). The signal intensities RCND-DTPA-Gd was proportional to the Gd concentration (0-0.12 mM). The longitudinal relaxivity (r_1) was measured as a value of 5.17 mM^{-1}·s^{-1}, and resulted significantly higher than Gd-DTPA (Magnevist, 3.40 mM^{-1}·s^{-1})[37] and similar to Gd-encapsulated carbon dots.[24] The enhanced r_1 was mainly explained with the high loading of gadolinium on the surface of the nanodots and their small dimension, which augmented the possibility of coordinating H_2O molecules owing to the increased surface-to-volume (*S*/*V*) ratio.[28] These data strongly support the use of

RCND-DTPA-Gd nanoparticles for MRI.

Knowing the high toxicity of free gadolinium, MRI agents containing the smallest amount of this element, while displaying high r_1, are still highly desirable. Some studies reported that Gd ions chelated on the surface of gadolinium-doped nanoparticles were the main responsible of the relaxation of water protons, while the same ions in the core of the nanoparticles did not contribute to a significant enhancement of relaxivity.[38] On the other side, the small size of the nanoparticles allowed to enhance longitudinal relaxivity because ultrasmall Gd-doped nanoparticles with a high specific surface area can maximize the dipole-dipole interactions between gadolinium atoms and protons, thus being responsible for high r_1.[39] In our case, our controlled method for synthesizing RCND-DTPA-Gd meets these requirements. Indeed, the functionalized RCND-DTPA-Gd displayed a high dispersibility, uniform small size, favorably interacting with water protons. The amount of gadolinium in RCND-DTPA-Gd was quantified by ICP-AES resulting 9.2±0.6% (w/w), which is significantly lower than previously reported carbon dot-based MRI agents.[24, 25, 39-41] Compared with the clinical contrast agent Magnevist, which owns a Gd content of 16.7%, RCND-DTPA-Gd shows a higher longitudinal relaxivity at a lower Gd content (9.2%). This suggests that RCND-DTPA-Gd likely have a better contact with water molecules than Magnevist. Since DTPA is able to form complexes with different transition metals, our nanocarrier RCND-DTPA could be easily exploited for the preparation of other types of metal-chelated RCNDs, including for example Mn^{2+}, Nd^{3+}, Eu^{3+} or ^{68}Ga.[42, 43] It is worth noting that there is the possibility to further improve *r1* relaxivity of CND-based MRI agents through a controlled modification of the CNDs with the chelating agent. Indeed, several factors can affect *r1* relaxivity, including the surface distribution and density of the chelating agents, the length and rigidity of the spacers, and water accessibility to Gd atoms. A chemical optimization of the synthesis could enhance the relaxivity values.[44]

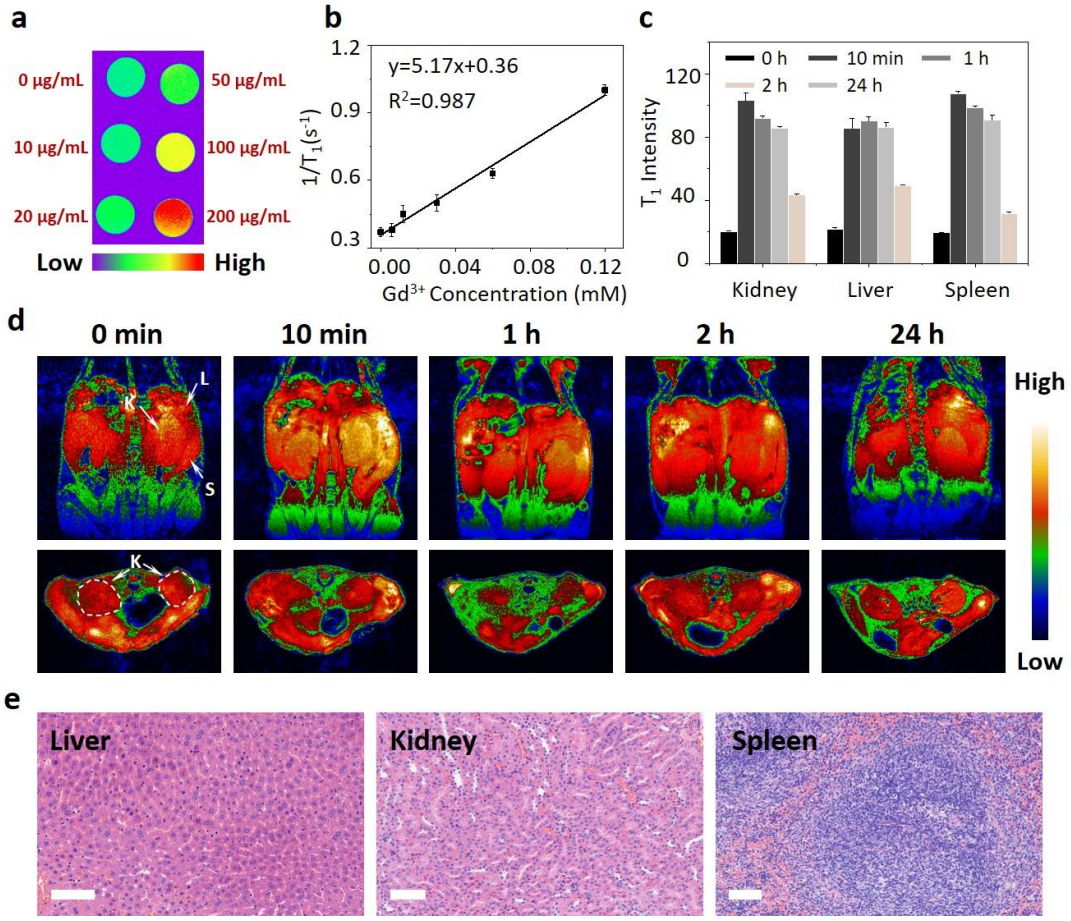

Figure 5. a) T_1-weighted phantom photographs of RCND-DTPA-Gd at different concentrations (0-200 μg·mL^{-1}); b) Linear correlation between r_1 (T_1^{-1}) and Gd concentration. r_1 relaxivity (the slope of the curve) corresponded to 5.17 mM^{-1}·s^{-1}; c) Quantification of signal variations in the kidney, spleen, and liver at different time points (0, 10 min, 1 h, 2 h, 24 h) after intravenous administration; d) MRI images of BALB/c mice after tail vain injection of RCND-DTPA-Gd (5 mg·kg^{-1}) obtained at different time points (L: liver, K: kidney, S: spleen); e) H&E images of the kidney, spleen, and liver after tail vein injection of RCND-DTPA-Gd (5 mg·kg^{-1}). The scale bar is 100 μm.

Biodistribution and *in vivo* imaging of RCND-DTPA-Gd

Assessing the biodistribution of the nanoparticles into the vital organs is fundamental in view of *in vivo* biomedical applications.[45] To monitor their organ biodistribution, RCND-DTPA-Gd nanoparticles were injected intravenously to mice and T_1-weighted images were recorded after 0 min, 10 min, 1 h, 2 h, and 24 h. The low dose of RCND-DTPA-Gd (5 mg·kg^{-1} body weight, corresponding to a gadolinium dose of 3

μmol·kg^{-1} body weight) generated a clear enhancement of the signal in the liver, spleen and kidney after 10 min post-injection (Figure 5c,d). In addition, we measured an increase of the signal in the bladder, indicating renal clearance of the injected nanodots (see Supplementary Video S1). There was also a signal increase throughout the abdominal cavity of the mice, followed by a decay starting from 2 h. After 24 h, the signals in most of the thoracic organs diminished to the levels before injection (Figure 5c,t has been wi

*d), indicating a rapid elimination of the nanodots from blood. The efficient kidney clearance was attributed to the small size of RCND-DTPA-Gd, in agreement with a previous report.[24] Furthermore, the histological analysis of the liver, spleen, and kidney indicated that the RCND-DTPA-Gd did not cause apparent damages of the tissues (Figure 5e).

It is widely recognized that high concentrations of nanoparticles easily lead to aggregates in the tissue, which would hamper their removal, provoking unpredictable toxicity.[46, 47] To evaluate the safety of the nanomaterials at a higher amount, we increased RCND-DTPA-Gd dose to a concentration of 20 mg·kg^{-1} (corresponding to a dose of gadolinium of 12 μmol·kg^{-1} body weight). As for the lower dose, we observed a similar distribution behavior of the nanoparticles in the main organs (Figure 6a, Supplementary Video S2). From the H&E staining images, we found no aggregates in the tissues suggesting a high biocompatibility. The high dose of RCND-DTPA-Gd caused no damage to the principal organs, including liver, spleen, kidney, heart, and lung (Figure 6b). This indicates that these highly biocompatible RCND-DTPA-Gd could be exploited for biomedical applications as alternative MRI contrast agents. Due to the great versatility in terms of surface modifications, the CNDs could be further conjugated with polyethylene glycol chains to prevent the formation of protein corona, thus extending blood circulation time *in vivo*, or by conjugating a targeting ligand to increase the level of intracellular uptake and bioavailability of the nanoparticles.[48]

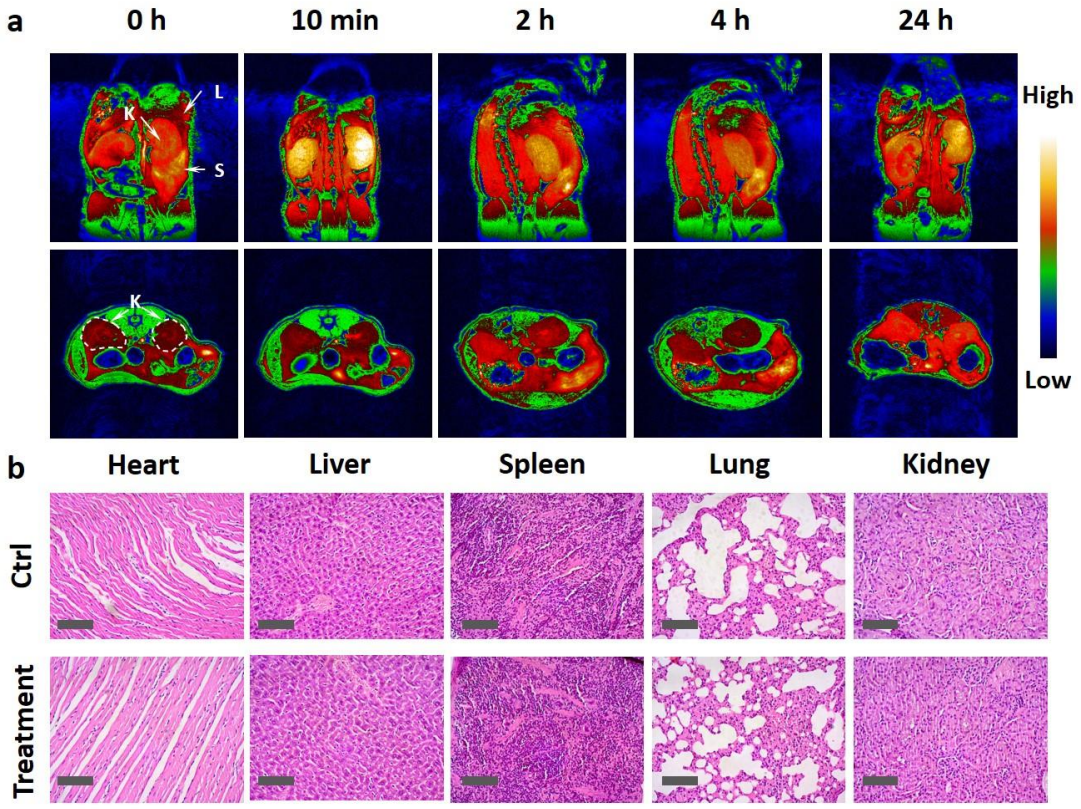

Figure 6. a) MRI images of BALB/c mice after tail vein injection of RCND-DTPA-Gd (20 mg·kg^{-1}) obtained at different time points (L: liver, K: kidney, S: spleen); b) H&E images of major organs after tail vein injection of RCND-DTPA-Gd (20 mg·kg^{-1}). The scale bar is 100 μm.

The chelation of gadolinium using different chelating agents and the stability of the complexes have been extensively studied many years ago.[49-51] It is worth noting that phosphate forms the insoluble salt $GdPO_4$, therefore any unchelated gadolinium will precipitate as insoluble salt in a phosphate buffer at pH 4. As Gd-DPTA (Magnevist) is clinically used and our carbon dot conjugates have exactly the same chemical chelating structure, we believe that the fast elimination is not a consequence of a Gd leakage, but of the rapid elimination of the conjugate itself.[24, 52, 53] Indeed, the DTPA-Gd moiety present on the RCNDs has the same structure than Magnevist, contrarily to most nanoparticles functionalized with DTPA in which one of the five carboxylic acids is converted to an amide bond using DTPA dianhydride.[30, 31] This synthetic approach is non-selective, due to the simultaneous formation of diamide derivatives, and results in generating less stable gadolinium complexes.[54] In our case, CND-DTPA has the benefit of presenting five free carboxylates available for efficient chelation of gadolinium.

Moreover, since its approval in 1988, Magnevist has been widely used for MRI in human. More recently, another DTPA-Gd based contrast agent (Gd-ethoxybenzyl-DTPA, Eovist or Primovist) received FDA approval for liver imaging applications in 2008.[44] Therefore, the stability of Gd chelated to DTPA has already been demonstrated. We would also like to highlight that the use of the xylenol orange test to prove the stability of DTPA-Gd complexes is strongly not recommended in PBS-containing solutions.[49, 50]

Biochemical analyses of RCND-DTPA

To further develop *ad-hoc* functionalized carbon nanodots for biological applications *in vivo*, we evaluated the impact of RCND-DTPA after intravenous administration in BALB/c mice on hematological and biochemical parameters of the animals. RCND-DTPA were injected intravenously with a dose of 10 $mg \cdot kg^{-1}$ body weight. Medical observations were done every day up to one month. All mice survived and no overall signs of toxicity were observed (*e.g.* immobility, disheveled hair, irregular respiration, gastrointestinal symptoms, seizures, convulsions, severe decubitus paralysis or death).

To evaluate the body toxicity of RCND-DTPA, a complete biochemical analysis of blood samples of BALB/c mice was performed after intravenous administration. Blood samples were collected at 24 h, 15 and 30 days, respectively. As shown in Table S1, normal values of urea and creatinine were found confirming that RCND-DTPA caused no toxic effects on renal function. Furthermore, the levels of AST, ALT, ALP, and creatinine remained normal, indicating a normal function of the liver.

Eventually, selected hematological parameters were evaluated to assess the hemocompatibility of RCND-DTPA (Table S2). All the parameters remained within the range of the control values showing no hematotoxicity caused by RCND-DTPA over 30 days, which makes this type of nanoparticles very promising for biomedical applications via systemic administration.

CONCLUSION

Overall, we have devised a simple and adaptable approach for the controlled functionalization of RCNDs with DTPA for chelation of gadolinium. The nanoparticles afforded high colloidal stability, strong red-emissive photoluminescence

and superior r_1 relaxivity compared to Magnevist. Remarkably, RCND-DTPA displayed no toxicity to mice and caused no damage to kidney and other organs. RCND-DTPA-Gd showed good biocompatibility *in vivo* even at a high dose and were efficiently excreted via the kidneys after systemic administration. All these advantages make RCND-DTPA-Gd an appealing MRI agent for clinical applications. Combining their far-red emissive photoluminescence and MRI capability, RCND-DTPA-Gd could also be exploited as *in vivo* dual MRI/fluorescence imaging probes, especially for imaging of soft tissues. This is a straightforward strategy for the covalent modification of carbon nanodots with DTPA. Considering the great versatility of their surface chemistry, RCNDs can be further modified to introduce multiple functions. This work is expected to promote the translation of carbon dots into clinical trials and opens up more opportunities for the development of next-generation carbon material-based nanomedicines.

MATERIALS AND METHODS

1. **Materials**

All chemicals used in the experiments were obtained from commercial sources as analytical reagents without further purification. 3-Thiophene boronic acid was purchased from Acros. Gadolinium(III) perchlorate 50% aqueous solution and xylenol orange were purchased from Sigma-Aldrich. *N*-hydroxysuccinimide (NHS) and 3-(4-bromophenyl) propanoic acid, 1-ethyl-3-(3-dimethylaminopropyl) carbodiimide hydrochloride (EDC·HCl) were purchased from Alfa Aesar. ^{1}H NMR spectra were recorded on Bruker DPX 300 instrument. The peak values were obtained as ppm (δ) and referenced to the solvent. The resonance multiplicity is indicated as s (singlet), d (doublet), t (triplet), dd (doublet of doublet), and m (multiplet). LC/MS analyses were performed on ThermoFisher Finnigan 6 LCQ Advantage Max. Centrifugation and bath sonication were performed on an Eppendorf centrifuge 5804R and an Elmasonic P sonicator. The dialysis was performed using membranes MWCO of 1 kDa from Spectrum Laboratories Inc. MilliQ water with a resistivity of 18.2 MΩ was used in the experiments.

2. Instruments for characterization of the materials

UV-Vis spectra were recorded using a VARIAN 5000 spectrometer. Fluorescence steady-state spectra were recorded via a Fluorolog FL3-22 (Horiba Jobin Yvon)

spectrometer using a swig xenon 450 W lamp. The FTIR spectra in KBr were collected on a Varian Excalibur 3100 FTIR spectrometer. Morphology of the samples was studied by HRTEM (JEM-2010F, JEOL, Japan). TGA was performed on a TGA1 (Mettler Toledo) apparatus from 100°C to 900°C with a ramp of 10°C·min^{-1} under N_2 atmosphere with a flow rate of 75 mL·min^{-1} and platinum pans. The DLS and zeta-potential measurements were done with a Zetasizer Nano ZS (Malvern, U.K.). XPS was performed using Thermo Scientific KAlpha X-ray spectrometer with a mono X-Ray source Al Kα excitation (1486 eV). Binding energy calibration was based on C1s at 284.7 eV. Inductively-coupled plasma atomic emission spectroscopy (ICP-AES) analyses were performed on a Thermo Flash 2000, Thermo Scientific. Photoluminescence quantum yield (PLQY) was performed on a FLS 1000, Edinburgh Instruments Ltd., and measured by a Hamamatsu Quantaurus-QY integrating sphere in air-equilibrated condition using an empty quartz tube as a reference.

HAADF-STEM images, EDX and EELS spectra and STEM-EELS spectrum images were acquired on a FEI Tecnai G2 F20 HR(S)TEM operated at 200 kV and equipped with an EDAX super ultra-thin window (SUTW) X-ray detector and a Gatan Quantum SE 963 imaging filter. Gd and C elemental maps were obtained by extracting the signal on the Gd $N_{4,5}$ and C K edges respectively. Samples were deposited on ultrathin carbon on holey carbon Cu TEM grids (TedPella).

3. Synthesis of red-emissive carbon nanodots

RCNDs were prepared by hydrothermal treatment of polythiophene phenylpropionic acidaccording to our previous work. [33] In brief, 20 mg of PPA was dispersed in 40 mL of NaOH solution (1 mM). The mixture was treated with bath sonication for 3 h and then transferred into an autoclave and heated at 220°C for a period of 24 h. After cooling to room temperature, the RCNDs were collected through filtering with 0.1-μm membranes for 3 times, and then dialyzed against distilled water for 5 days to remove the residual NaOH. After lyophilization, a red solid was obtained.

4. Synthesis of DTPA ligand

DTPA ligand was prepared according to our previous work (Scheme S1).[19]

Synthesis of 6-benzyloxycarbonylamino-2-{bis-[2-(bis-tert-butoxycarbonyl-methyl-amino)-ethyl]-amino}-hexanoic acid tert-butyl ester (2).

The compound **2** was prepared according to our previous work.[19]

^{1}H NMR (400 MHz, $CDCl_3$) δ 7.38-7.27 (m, 5H), 5.20-4.98 (m, ,3H), 3.42 (s, 8H) 3.27-3.08 (m, 3H) 2.97-2.48 (m, 8H), 1.43 (s, 51H). ^{13}C NMR (500 MHz, $CDCl_3$) δ 170.63, 156.44, 136.77, 128.44, 128.10, 127.96, 80.87, 66.41, 63.97, 55.91, 53.56, 50.25, 40.80, 29.40, 28.28, 28.17, 23.45. LC-MS (ESI): m/z 879.35 $[M+H]^+$.

Synthesis of 6-amino-2-{bis-[2-(bis-*tert*-butoxycarbonyl-methyl-)-ethyl]-amino}-hexanoic acid *tert*-butyl ester (3). A catalytic amount of Pd/C (20 mg) was added to a solution of compound 1 (240 mg) in methanol (10 mL). The mixture was stirred under a hydrogen atmosphere at room temperature for 5 h. The suspension was filtered twice with filter paper to remove residual Pd/C. Then the filtrate was concentrated under vacuum and purified by chromatography on silica gel using DCM/MeOH from 20/1 to 5/1 as eluant. 156 mg of compound was obtained as colorless oil. (Yield is 77%). ^{1}H NMR (400 MHz, MeOD) δ 3.42 (s, 8H), 3.40 – 3.33 (m, 1H), 2.99 – 2.91 (m, 2H), 2.85 – 2.73 (m, 6H), 2.72 – 2.60 (m, 2H), 1.76 – 1.60 (m, 4H), 1.54 – 1.43 (m, 47H). ^{13}C NMR (500 MHz, MeOD) δ 174.14, 172.36, 82.46, 64.87, 57.22, 54.42, 50.82, 40.74, 29.81, 28.63, 28.52, 28.30, 24.37. LC-MS (ESI): m/z 745.34 $[M+H]^+$.

5. Conjugation of DTPA ligand to RCNDs

A suspension of RCND (8 mg) in DI water (8 mL) was sonicated in an ice bath for 10 min. NHS (80 mg, mmol), EDC·HCl (128 mg), and trimethylamine (192 μL) were added, and the mixture was stirred for 4 h. Afterwards, a solution of **3** (24 mg) in DMSO (0.8 mL) was carefully added and then stirred for another 20 h at room temperature. The mixture was dialyzed (1 kDa membrane) against DI water for 3 days. After lyophilization, a red solid (15 mg) was obtained.

6. Preparation of RCND-DTPA

Fifteen mg of functionalized RCNDs were added to 3 mL DI water to form a red suspension. After sonication for 10 min, 3 mL of TFA were added dropwise to the suspension in an ice bath. Then, the suspension was stirred at room temperature for 24 h. The residues were removed through dialysis with 1 KDa membrane against DI water for 2 days. The suspension was lyophilized to obtain 7.5 mg RCND-DTPA.

7. Preparation of RCND-DTPA-Gd

Gadolinium(III) perchlorate 50% aqueous solution was added to a suspension of RCND-DTPA (6 mg) to form a dark red solution. After sonication for 10 min, the solution was stirred for 20 h at room temperature. The unchelated Gd was removed via membrane dialysis (1 kDa) in DI water for 2 days. The suspension was lyophilized to obtain RCND-DTPA-Gd. All biological experiments were performed using the same batch of material.

8. Calculations of the amount of Gd atoms per C atoms[55]

According to XPS, RCND-DTPA-Gd contains 75.85 %C, 14.05 %O, 5.77 %S, 3.97 %N, 0.37 % Gd. The molecular weight of RCND-DTPA-Gd was estimated: 0.7585*12 + 0.1405*16 + 0.0577*32 + 0.0397*14 + 0.0037*157= 14.33 g/mol.

Therefore, the weight % of carbon atoms in RCNDs-DTPA-Gd is: 100*(0.7585*12)/14.33 = 63.52 wt% C. One g of RCND-DTPA-Gd contains 0.635 g of carbon atoms (52.9 mmol). For the value of 586 μmol (from ICP-AES) of Gd per gram of RCND-DTPA-Gd, we found that there is one Gd atom every 90 C atoms (52.9/0.586).

9. UV-Vis-NIR and fluorescence spectroscopy of RCND, RCND-DTPA, RCND-DTPA-Gd

RCND, RCND-DTPA, RCND-DTPA-Gd at a concentration of 25 $\mu g \cdot mL^{-1}$ were added to 0.01 M PBS (pH=7.4, without Ca^{2+} and Mg^{2+}). After bath sonication for 5 min, their UV-Vis-NIR and fluorescence spectroscopy were measured at room temperature.

10. DLS and zeta-potential measurements of RCNDs, RCND-DTPA, RCND-DTPA-Gd

RCNDs, RCND-DTPA, RCND-DTPA-Gd at a concentration of 25 $\mu g \cdot mL^{-1}$ were added to 0.01 M PBS (pH=7.4, without Ca^{2+} and Mg^{2+}), and sonicated for 15 min to form a stable colloidal solution. The size distribution and surface charge of each sample were obtained by a Zetasizer nano (Malvern Instruments, Malvern, UK).

11. Relaxivity measurements

The *in vitro* MR imaging experiments were performed in a 7 T clinical MRI scanner (Bruker Biospoin GmbH, Germany). RCND-DTPA-Gd samples were dispersed in

water at various sample concentrations (0, 10, 20, 50, 100, 200 μg·mL^{-1}). T_1 was acquired using an inversion recovery sequence. T_1 measurements were performed using a nonlinear fit to changes in the mean signal intensity within each well as a function of repetition time (TR). Finally, the r_1 relaxivity values were determined through the curve fitting of $1/T_1$ relaxation time (s^{-1}) versus the Gd concentration in the samples. The relaxivity can be written as shown in equation (1).

$$\frac{1}{T1} = \frac{1}{T2} + r_1[Gd] \quad (1)$$

Table 1: Data for r_1 relaxivity curve.

RCND-DTPA-Gd （μg·mL^{-1}）	0	10	20	50	100	200
Gd (mM)	0	0.006	0.012	0.03	0.06	0.12
Relaxation time (s)	2.7	2.6	2.2	2.0	1.6	1.0
$1/T_1$ (s^{-1})	0.37	0.38	0.45	0.5	0.625	1

12. Cell culture

HeLa (epithelial, human cervical adenocarcinoma) cells were cultured as monolayers in Dulbecco's modified Eagle medium (DMEM) supplemented with 10 μg·mL^{-1} gentamycin, 10 mM *N*-(2-hydroxyethyl)-piperazine-*N*-ethanesulfonic acid, 0.05 mM β-mercaptoethanol, and 10% fetal bovine serum (FBS) at 37℃ in a 5% CO_2 incubator.

13. Cytotoxicity assay

The cytotoxicity of RCND-DTPA-Gd was tested on the HeLa cell line using Prestoblue reagent. HeLa cells were incubated in 96-well culture plates at a density of 2000 cells per well in culture medium at 37℃ for 24 h. RCND-DTPA-Gd at varying concentrations (0, 10, 25, 50, 75, 100 μg·mL^{-1}) were added to cells and incubated for another 24 h. The culture media were discarded, and 0.1 mL of the Prestoblue solution (10% in cell medium) was added to each well, followed by incubation at 37℃ for 2 h. Absorbance values of the wells were read with a microplate reader (Thermo Scientific, Multiskan FC) at 570 nm and 620 nm. The experiment was performed under identical conditions for three times.

14. Cell imaging and assessment of particle endocytosis

For fluorescence imaging, the adherent HeLa cells grown on glass-bottom culture dishes containing 0.5 mL of culture medium were first incubated with CellMask (Sigma-Aldrich) for 2 h. After washing with cell culture medium 2 times, the cell lines were incubated with RCND-DTPA-Gd (50 $\mu g \cdot mL^{-1}$) for 24 h at 37°C. The fluorescence images were taken at 0, 4 h, 8 h, and 24 h.

Confocal images were obtained with a Zeiss Axio Observer Z1 spinning disk confocal microscope equipped with 100 X oil objective. The fluorescence signal from CellMask was obtained using a 488 nm laser excitation and recorded in the green channel (505-555 nm), whereas RCND-DTPA-Gd were recorded using a 405 nm laser excitation in the far-red (FR) channel (665-715 nm). Images were then treated with ImageJ software.

15. Animal experiments and MRI protocols

The doses injected were approved by the Ethics Committees (see below) and they are in the range of most of *in vivo* biodistribution studies that involve carbon nanomaterials.

General toxicity. Toxicological characterization of RCND-DTPA after a single intravenous administration was performed in a murine model (BALB/c mice, 11-13 weeks, 18-20 g, n=5/group). Mice were housed in the IBMC animal facility (agreement number G67-482-2). They were maintained under controlled conditions before and during the experiments (*i.e.*, room temperature at 25°C; relative humidity of 65%; 12 h light/dark cycle). Access to food and water was provided *ad libitum*. All experiments were carried out in conformity with the 2010/63/UE European animal bioethics legislation (French decree #2013-118 – 1st February 2013) and were approved by the Regional Ethics Committee of Strasbourg (CREMEAS) and by the French Ministry of Higher Education and Research (APAFIS#3280-2015121815099907v2). An acute toxicity assay was performed using RCND-DTPA at the dose of 10 $mg \cdot kg^{-1}$ body weight (injections of 200 µg/mouse, respectively). After a single intravenous injection of RCND-DTPA PBS solution, clinical observations were performed daily up to 30 days. Animals were sacrificed at 24 h, 14 and 30 days after. Blood was collected in EDTA (10%) and analyzed using a Cell Counter. The biochemical and hematological analyses were performed at the Mouse Clinical Institute (MCI, Illkirch, France).

T_1-weighted MR imaging

Male BALB/c nude mice (20~22 g) were obtained from Jie Si Jie Laboratory Animals (Shanghai, China). All mice were bred in the animal facility of Renji Hospital according to the Guide for the Care and Use of Laboratory Animals. The entire study was approved by the Institutional Animal Care Committee of Renji Hospital. For the low-dose T_1-weighted MR imaging *in vivo*, the mice were intravenously injected with the RCND-DTPA-Gd PBS solution at the dose of 100 μg RCND-DTPA-Gd per mouse (5 mg·kg^{-1}) (n = 3). T_1-weighted MR scanning images were obtained using a 7.0 T clinical MRI scanner (Bruker Biospoin GmbH, Germany) at different injection time points (0, 10 min, 1 h, 2 h, 24 h). All the MR scanning images were performed with the same parameter settings.

For the high-dose T_1-weighted MR imaging *in vivo*, the mice were intravenously injected with the RCND-DTPA-Gd solution at the dose of 400 μg CND-DTPA-Gd per mouse (20 mg·kg^{-1}) (n = 3). T_1-weighted MR scanning images were obtained using a 7.0 T MRI scanner (Bruker Biospoin GmbH, Germany) for 0, 10 min, 2 h, 4 h, 24 h, respectively. Dimeglumine gadopentetate at the same Gd dose (Magnevist, a commercial MRI contrast agent) was used as a control. T_1-weighted MR imaging was performed using an inversion recovery gradient echo sequence with TE = 4 ms, a slice thickness of 0.5 mm, a field of view (FOV) of 3.0 × 3.0 cm, and a matrix size of 128 × 128.

Organ histology

After excision, pieces of heart, liver, spleen, lung, and kidney were fixed with pH 7.4 phosphate-buffered 10% formalin and processed by embedding in paraffin. Sections, ~6 μm thick, were evaluated by a Zeiss microscope (Axio Lab.A1) after staining with hematoxylin and eosin (H&E).

ASSOCIATED CONTENT

Supporting Information

The Supporting Information is available free of charge at https://pubs.acs.org/doi/10.1021/acsanm.0c02993.

Organ distribution of RCND-DTPA-Gd in vivo (Videos S1 and S2) (ZIP).

Synthesis of DTPA ligand (Scheme S1), additional HAADF-STEM images of the RCND-DTPA-Gd sample (Figure S1), DLS of RCND-DTPA-Gd (Figure S2), FL spectra of CND-DTPA-Gd (Figure S3), cell viability of RCND-DTPA-Gd (Figure S4), organ distribution of RCND-DTPA-Gd in vivo (Videos S1 and S2), and the hematological and biochemical parameters of RCND-DTPA (Tables S1 and S2) (PDF).

AUTHOR INFORMATIONS

Corresponding Authors

E-mail: a.bianco@ibmc-cnrs.unistra.fr

ORCID

Cécilia Ménard-Moyon: 0000-0003-0348-2466

Giacomo Reina: 0000-0002-8147-3162

Alberto Bianco: 0000-0002-1090-296X

ACKNOWLEDGMENTS

We gratefully acknowledge the Centre National de la Recherche Scientifique (CNRS), the International Center for Frontier Research in Chemistry (icFRC), and financial support from the Agence Nationale de la Recherche (ANR) through the LabEx project Chemistry of Complex Systems (ANR-10-LABX-0026_CSC) within the Investissement d'Avenir program (ANR-10-120 IDEX-0002-02). We wish to thank D. Lamon for injecting the mice and collecting the samples for the biochemical analyses, C. Royer and V. Demais for help with TEM analyses at the "Plateforme Imagerie in vitro" at the Center of Neurochemistry (INCI, Strasbourg, France), D. Ihiawakrim for HRTEM measurements, and S. Guo for his help in the XPS analyses. ICN2

acknowledges financial support from the Spanish Ministry of Economy and Competitiveness, through the “Severo Ochoa” Programme for Centres of Excellence in R&D (SEV-2017-0706). BB acknowledges funding from Generalitat de Catalunya 2017 SGR 327. We wish to thank the Academy of Integrative Medicine, Fujian University of Traditional Chinese Medicine, Fujian Key Laboratory of Integrative Medicine on Geriatrics, and Prof. Jun Peng for the use of 7T small animal MRI scanner.

REFERENCES

(1) Terreno, E.; Castelli, D. D.; Viale, A.; Aime, S. Challenges for Molecular Magnetic Resonance Imaging. *Chem. Rev.* **2010**, *110* , 3019–3042.

(2) Kim, J.; Piao, Y.; Hyeon, T. Multifunctional Nanostructured Materials for Multimodal Imaging, and Simultaneous Imaging and Therapy. *Chem. Soc. Rev.* **2009**, *38* , 372–390.

(3) Penfield, J. G.; Reilly, R. F. What Nephrologists Need to Know about Gadolinium. *Nat. Clin. Pract. Nephrol.* **2007**, *3*, 654–668.

(4) Chrysochou, C.; Power, A.; Shurrab, A. E.; Husain, S.; Moser, S.; Lay, J.; Salama, A. D.; Kalra, P. A. Low Risk for Nephrogenic Systemic Fibrosis in Nondialysis Patients Who Have Chronic Kidney Disease and Are Investigated with Gadolinium-Enhanced Magnetic Resonance Imaging. *Clin. J. Am. Soc. Nephrol.* **2010**, *5*, 484–489.

(5) Hellman, R. N. Gadolinium-Induced Nephrogenic Systemic Fibrosis. *Semin. Nephrol.* **2011**, *31*, 310–316.

(6) Na, H. Bin; Song, I. C.; Hyeon, T. Inorganic Nanoparticles for MRI Contrast Agents. *Adv. Mater.* **2009**, *21*, 2133–2148.

(7) Ni, D.; Bu, W.; Ehlerding, E. B.; Cai, W.; Shi, J. Engineering of Inorganic Nanoparticles as Magnetic Resonance Imaging Contrast Agents. *Chem Soc Rev* **2018**, *46*, 7438–7468.

(8) Deka, K.; Guleria, A.; Kumar, D.; Biswas, J.; Lodha, S.; Kaushik, S. D.; Choudhary, S. A.; Dasgupta, S.; Deb, P. Janus Nanoparticles for Contrast Enhancement of T_1–T_2 Dual Mode Magnetic Resonance Imaging. *Dalt. Trans.* **2019**, *48*, 1075–1083.

(9) Saha, A.; Mohanta, S. C.; Deka, K.; Deb, P.; Devi, P. S. Surface-Engineered Multifunctional Eu : Gd_2O_3 Nanoplates for Targeted and PH-Responsive Drug Delivery and Imaging Applications. *ACS Appl. Mater. Interfaces* **2017**, *9* (4), 4126–4141.

(10) Mao, X.; Xu, J.; Cui, H. Functional Nanoparticles for Magnetic Resonance Imaging. *Wiley Interdiscip. Rev. Nanomedicine Nanobiotechnology* **2016**, *8*, 814–841.

(11) Yon, M.; Billotey, C.; Marty, J.-D. Gadolinium-Based Contrast Agents: From Gadolinium Complexes to Colloidal Systems. *Int. J. Pharm.* **2019**, *569*, 118577.

(12) Yang, H.; Qin, C.; Yu, C.; Lu, Y.; Zhang, H.; Xue, F.; Wu, D.; Zhou, Z.; Yang, S. RGD-Conjugated Nanoscale Coordination Polymers for Targeted T_1-and T_2-Weighted Magnetic Resonance Imaging of Tumors *in Vivo*. *Adv. Funct. Mater.* **2014**, *24*, 1738–1747.

(13) Vivero-Escoto, J. L.; Taylor-Pashow, K. M. L.; Huxford, R. C.; Della Rocca, J.; Okoruwa, C.; An, H.; Lin, W.; Lin, W. Multifunctional Mesoporous Silica Nanospheres with Cleavable Gd (III) Chelates as MRI Contrast Agents: Synthesis, Characterization, Target-Specificity, and Renal Clearance. *Small*

2011, *7*, 3519–3528.

(14) Zhang, G.; Gao, J.; Qian, J.; Zhang, L.; Zheng, K.; Zhong, K.; Cai, D.; Zhang, X.; Wu, Z. Hydroxylated Mesoporous Nanosilica Coated by Polyethylenimine Coupled with Gadolinium and Folic Acid: A Tumor-Targeted T_1 Magnetic Resonance Contrast Agent and Drug Delivery System. *ACS Appl. Mater. Interfaces* **2015**, *7*, 14192–14200.

(15) Vivero-Escoto, J. L.; Rieter, W. J.; Lau, H.; Huxford-Phillips, R. C.; Lin, W. Biodegradable Polysilsesquioxane Nanoparticles as Efficient Contrast Agents for Magnetic Resonance Imaging. *Small* **2013**, *9*, 3523–3531.

(16) Ananta, J. S.; Godin, B.; Sethi, R.; Moriggi, L.; Liu, X.; Serda, R. E.; Krishnamurthy, R.; Muthupillai, R.; Bolskar, R. D.; Helm, L. Geometrical Confinement of Gadolinium-Based Contrast Agents in Nanoporous Particles Enhances T_1 Contrast. *Nat. Nanotechnol.* **2010**, *5*, 815–821.

(17) Sitharaman, B.; Kissell, K. R.; Hartman, K. B.; Tran, L. A.; Baikalov, A.; Rusakova, I.; Sun, Y.; Khant, H. A.; Ludtke, S. J.; Chiu, W. Laus, S.; Toth, E.; Helm, L.; Merbachd, A. E.; Wilson, L. J.. Superparamagnetic Gadonanotubes Are High-Performance MRI Contrast Agents. *Chem. Commun.* **2005**, *31*, 3915–3917.

(18) Rodríguez-Galván, A.; Rivera, M.; García-López, P.; Medina, L. A.; Basiuk, V. A. Gadolinium-containing Carbon Nanomaterials for Magnetic Resonance Imaging: Trends and Challenges. *J. Cell. Mol. Med.* **2020**, *24* (7), 3779–3794.

(19) Marangon, I.; Ménard-Moyon, C.; Kolosnjaj-Tabi, J.; Béoutis, M. L.; Lartigue, L.; Alloyeau, D.; Pach, E.; Ballesteros, B.; Autret, G.; Ninjbadgar, T.; Brougham, Dermot F. Bianco, A.; Gazeau, F. Covalent Functionalization of Multi-Walled Carbon Nanotubes with a Gadolinium Chelate for Efficient T_1-Weighted Magnetic Resonance Imaging. *Adv. Funct. Mater.* **2014**, *24*, 7173-7186.

(20) Xu, X.; Ray, R.; Gu, Y.; Ploehn, H. J.; Gearheart, L.; Raker, K.; Scrivens, W. A. Electrophoretic Analysis and Purification of Fluorescent Single-Walled Carbon Nanotube Fragments. *J. Am. Chem. Soc.* **2004**, *126*, 12736–12737.

(21) Lim, S. Y.; Shen, W.; Gao, Z. Carbon Quantum Dots and Their Applications. *Chem. Soc. Rev.* **2015**, *44*, 362–381.

(22) Du, J.; Xu, N.; Fan, J.; Sun, W.; Peng, X. Carbon Dots for In Vivo Bioimaging and Theranostics. *Small* **2019**, *15*, 1805087.

(23) Liu, J.; Li, R.; Yang, B. Carbon Dots: A New Type of Carbon-Based Nanomaterial with Wide Applications. *ACS Cent. Sci.* **2020**, *6*, 2179.

(24) Chen, H.; Wang, G. D.; Tang, W.; Todd, T.; Zhen, Z.; Tsang, C.; Hekmatyar, K.; Cowger, T.; Hubbard, R. B.; Zhang, W.; Stickney, John.; Xie, J. Gd-Encapsulated Carbonaceous Dots with Efficient Renal Clearance for Magnetic Resonance Imaging. *Adv. Mater.* **2014**, *26*, 6761–6766.

(25) Bourlinos, A. B.; Bakandritsos, A.; Kouloumpis, A.; Gournis, D.; Krysmann, M.; Giannelis, E. P.; Polakova, K.; Safarova, K.; Hola, K.; Zboril, R.

Gd(III)-Doped Carbon Dots as a Dual Fluorescent-MRI Probe. *J. Mater. Chem.* **2012**, *22*, 23327.

(26) Atabaev, T.; Piao, Z.; Molkenova, A. Carbon Dots Doped with Dysprosium: A Bimodal Nanoprobe for MRI and Fluorescence Imaging. *J. Funct. Biomater.* **2018**, *9*, 35.

(27) Xu, Y.; Jia, X.; Yin, X.; He, X.; Zhang, Y. Carbon Quantum Dot Stabilized Gadolinium Nanoprobe Prepared via a One-Pot Hydrothermal Approach for Magnetic Resonance and Fluorescence Dual-Modality Bioimaging. *Anal. Chem.* **2014**, *86*, 12122–12129.

(28) Zhao, Y.; Hao, X.; Lu, W.; Wang, R.; Shan, X.; Chen, Q.; Sun, G.; Liu, J. Facile Preparation of Double Rare Earth-Doped Carbon Dots for MRI/CT/FI Multimodal Imaging. *ACS Appl. Nano Mater.* **2018**, *1*, 2544–2551.

(29) Gao, A.; Kang, Y.; Yin, X. Red Fluorescence-Magnetic Resonance Dual Modality Imaging Applications of Gadolinium Containing Carbon Quantum Dots with Excitation Independent Emission. *New J. Chem.* **2017**, *41*, 3422–3431.

(30) Shi, Y.; Pan, Y.; Zhong, J.; Yang, J.; Zheng, J.; Cheng, J.; Song, R.; Yi, C. Facile Synthesis of Gadolinium (III) Chelates Functionalized Carbon Quantum Dots for Fluorescence and Magnetic Resonance Dual-Modal Bioimaging. *Carbon* **2015**, *93*, 742–750.

(31) Du, Y.; Qian, M.; Li, C.; Jiang, H.; Yang, Y.; Huang, R. Facile Marriage of Gd^{3+} to Polymer-Coated Carbon Nanodots with Enhanced Biocompatibility for Targeted MR/Fluorescence Imaging of Glioma. *Int. J. Pharm.* **2018**, *552*, 84–90.

(32) Hnatowich, D. J.; Layne, W. W.; Childs, R. L. The Preparation and Labeling of DTPA-Coupled Albumin. *Int. J. Appl. Radiat. Isot.* **1982**, *33*, 327–332.

(33) Ji, D.-K.; Reina, G.; Guo, S.; Eredia, M.; Samorì, P.; Ménard-Moyon, C.; Bianco, A. Controlled Functionalization of Carbon Nanodots for Targeted Intracellular Production of Reactive Oxygen Species. *Nanoscale Horizons* **2020**, *5*, 1240–1249.

(34) Anelli, P. L.; Fedeli, F.; Gazzotti, O.; Lattuada, L.; Lux, G.; Rebasti, F. L-Glutamic Acid and L-Lysine as Useful Building Blocks for the Preparation of Bifunctional DTPA-like Ligands. *Bioconjug. Chem.* **1999**, *10*, 137–140.

(35) Richard, C.; Doan, B.; Beloeil, J.; Bessodes, M.; Tóth, É.; Scherman, D. Noncovalent Functionalization of Carbon Nanotubes with Amphiphilic Gd^{3+} Chelates: Toward Powerful T_1 and T_2 MRI Contrast Agents. *Nano Lett.* **2008**, *8*, 232–236.

(36) Zhang, S.; Gao, H.; Bao, G. Physical Principles of Nanoparticle Cellular Endocytosis. *ACS Nano* **2015**, *9*, 8655–8671.

(37) Yang, Z.; He, W.; Zheng, H.; Wei, J.; Liu, P.; Zhu, W.; Lin, L.; Zhang, L.; Yi, C.; Xu, Z.; Ren, J. One-Pot Synthesis of Albumin-Gadolinium Stabilized Polypyrrole Nanotheranostic Agent for Magnetic Resonance Imaging Guided

Photothermal Therapy. *Biomaterials* **2018**, *161*, 1–10.
(38) Johnson, N. J. J.; Oakden, W.; Stanisz, G. J.; Scott Prosser, R.; van Veggel, F. C. J. M. Size-Tunable, Ultrasmall $NaGdF_4$ Nanoparticles: Insights into Their T_1 MRI Contrast Enhancement. *Chem. Mater.* **2011**, *23*, 3714–3722.
(39) Gong, N.; Wang, H.; Li, S.; Deng, Y.; Chen, X.; Ye, L.; Gu, W. Microwave-Assisted Polyol Synthesis of Gadolinium-Doped Green Luminescent Carbon Dots as a Bimodal Nanoprobe. *Langmuir* **2014**, *30*, 10933–10939.
(40) Ren, X.; Liu, L.; Li, Y.; Dai, Q.; Zhang, M.; Jing, X. Facile Preparation of Gadolinium (III) Chelates Functionalized Carbon Quantum Dot-Based Contrast Agent for Magnetic Resonance/Fluorescence Multimodal Imaging. *J. Mater. Chem. B* **2014**, *2*, 5541–5549.
(41) Huang, C.-L.; Huang, C.-C.; Mai, F.-D.; Yen, C.-L.; Tzing, S.-H.; Hsieh, H.-T.; Ling, Y.-C.; Chang, J.-Y. Application of Paramagnetic Graphene Quantum Dots as a Platform for Simultaneous Dual-Modality Bioimaging and Tumor-Targeted Drug Delivery. *J. Mater. Chem. B* **2015**, *3*, 651–664.
(42) Clough, T. J.; Jiang, L.; Wong, K.-L.; Long, N. J. Ligand Design Strategies to Increase Stability of Gadolinium-Based Magnetic Resonance Imaging Contrast Agents. *Nat. Commun.* **2019**, *10*, 1420.
(43) Chinen, L. K.; Galen, K. P.; Kuan, K. T.; Dyszlewski, M. E.; Ozaki, H.; Sawai, H.; Pandurangi, R. S.; Jacobs, F. G.; Dorshow, R. B.; Rajagopalan, R. Fluorescence-Enhanced Europium-Diethylenetriaminepentaacetic (DTPA)-Monoamide Complexes for the Assessment of Renal Function. *J. Med. Chem.* **2008**, *51*, 957–962.
(44) Wahsner, J.; Gale, E. M.; Rodríguez-Rodríguez, A.; Caravan, P. Chemistry of MRI Contrast Agents: Current Challenges and New Frontiers. *Chem. Rev.* **2019**, *119*, 957–1057.
(45) Kurapati, R.; Kostarelos, K.; Prato, M.; Bianco, A. Biomedical Uses for 2D Materials Beyond Graphene: Current Advances and Challenges Ahead. *Adv. Mater.* **2016**, *28*, 6052–6074.
(46) Sukhanova, A.; Bozrova, S.; Sokolov, P.; Berestovoy, M.; Karaulov, A.; Nabiev, I. Dependence of Nanoparticle Toxicity on Their Physical and Chemical Properties. *Nanoscale Res. Lett.* **2018**, *13*, 44.
(47) Yildirimer, L.; Thanh, N. T. K.; Loizidou, M.; Seifalian, A. M. Toxicology and Clinical Potential of Nanoparticles. *Nano Today* **2011**, *6*, 585–607.
(48) Wang, B.; He, X.; Zhang, Z.; Zhao, Y.; Feng, W. Metabolism of Nanomaterials in *Vivo* : Blood Circulation and Organ Clearance. *Acc. Chem. Res.* **2013**, *46*, 761–769.
(49) Bingler, L. S.; Byrne, R. H. Phosphate Complexation of Gadolinium(III) in Aqueous Solution. *Polyhedron* **1989**, *8*, 1315–1320.
(50) Sherry, A. D.; Caravan, P.; Lenkinski, R. E. Primer on Gadolinium Chemistry. *J. Magn. Reson. Imaging* **2009**, *30*, 1240–1248.

(51) Rogosnitzky, M.; Branch, S. Gadolinium-Based Contrast Agent Toxicity: A Review of Known and Proposed Mechanisms. *BioMetals* **2016**, *29*, 365–376.
(52) Chen, H.; Wang, G. D.; Sun, X.; Todd, T.; Zhang, F.; Xie, J.; Shen, B. Gd Carbon Dots: Mesoporous Silica as Nanoreactors to Prepare Gd-Encapsulated Carbon Dots of Controllable Sizes and Magnetic Properties. *Adv. Funct. Mater.* **2016**, *26*, 4036–4036.
(53) Su, Y.; Liu, S.; Guan, Y.; Xie, Z.; Zheng, M.; Jing, X. Renal Clearable Hafnium-Doped Carbon Dots for CT/Fluorescence Imaging of Orthotopic Liver Cancer. *Biomaterials* **2020**, *255*, 120110.
(54) Sherry, A. D.; Cacheris, W. P.; Kuan, K.-T. Stability Constants for Gd^{3+} Binding to Model DTPA-Conjugates and DTPA-Proteins: Implications for Their Use as Magnetic Resonance Contrast Agents. *Magn. Reson. Med.* **1988**, *8*, 180–190.
(55) Vacchi, I. A.; Guo, S.; Raya, J.; Bianco, A.; Ménard-Moyon, C. Strategies for the Controlled Covalent Double Functionalization of Graphene Oxide. *Chem. – A Eur. J.* **2020**, *26*, 6591–6598.

Graphical Abstract